Instituto de Ciências Matemáticas de São Carlos

ISSN - 0103-2577

On the bifurcation [illegible] of general two dimensional spatial motions

C.G. GIBSON
C.A. HOBBS
W.L. MARAR

No. 32

NOTAS DO ICMSC
Série Matemática

São Carlos
Nov./1995

RESUMO

Fornecemos os modelos locais das singularidades que podem aparecer em trajetórias de movimentos bi-dimensionais gerais no espaço. Desdobramentos versais destas singularidades dão origem a figuras as quais descrevem a família de trajetórias que surgem de pequenas pertubações do ponto em movimento.

On the Bifurcation of General Two–Dimensional Spatial Motions[1]

C. G. Gibson
Department of Pure Mathematics, University of Liverpool,
PO Box 147, Liverpool, L69 3BX, England.

C. A. Hobbs[2]
School of Computing & Mathematical Sciences, Oxford Brookes University,
Gipsy Lane, Headington, Oxford, OX3 0BP, England.

W. L. Marar[3]
ICMSC, Universidade de São Paulo,
Caixa Postal 668, 13560 São Carlos (SP), Brazil

November 10, 1995

Abstract

Local models are given for singularities which can appear on the trajectories of general two-dimensional spatial motions. Versal unfoldings of these model singularities give rise to computer generated pictures describing the family of trajectories arising from small deformations of the tracing point. [4]

[1]Short Title: Bifurcation of Two–Dimensional Spatial Motions.

[2]The second author gratefully acknowledges financial support from the Science and Engineering Research Council.

[3]W. L. Marar acknowledges financial support from CNPq.

[4]AMS 1991 Classification: 70B10, 57R45

1 Introduction

This paper is the third in a series [3, 4] devoted to a very basic question in theoretical kinematics, of considerable potential importance in engineering robotics. The question is that of describing the surprisingly complex geometry associated to singularities of trajectories for *general* motions of the plane and space. In [3] the first two authors used standard techniques of Singularity Theory to establish that for general one-parameter motions of the plane and space there is a finite list of models for the local behaviour of trajectories. Versal unfoldings of these models then yield complete descriptions of the behaviour resulting from small changes in the position of the tracing point. One-parameter motions of the plane are relatively well understood geometric objects, and the resulting pictures do little more than confirm the kind of instincts which a working engineer is likely to have: rather less is understood about one-parameter motions of space, and already the pictures throw up objects which do not appear to have been studied in the established literature.

The question changes quite dramatically however when one moves forward to the multi-parameter motions of the plane and space, closer to the daily concern of working kinematicians. In this paper we set out to describe local models associated to general two-dimensional motions of space. Here the trajectories are surfaces in 3-space, whose singularities can describe a range of very complex behaviour. A key point is that the changes in the models obtained by small perturbations of the tracing point are described by the versal unfoldings of the local models. It takes an exceptional geometric 'feel' to guess even the simplest kinds of picture which can arise: thus there is little question that the mathematical analysis really has something to offer the working kinematician, especially since the interface is a graphical one. In fact the pictures are on the edge of what can (realistically) be done by hand. We found it helpful, and in some cases necessary, to study the surfaces in question on a dedicated graphics workstation. (Silicon Graphics IRIS 4D70GT.) Insight into the geometry of the double point curve was provided in some cases via the program ALGCURVE developed by our colleague Dr. R. Morris from a public domain program for tracing plane algebraic curves. His program ALGSURF, which produces rotatable images of algebraic surfaces, proved to be invaluable in checking our analyses of several of the surfaces which appear in our work, and in some cases even suggested further lines of investigation.

One of the interesting mathematical questions which arises from this study is whether all the local models we describe can actually be exhibited mechanically. Very few examples of coupler surfaces have ever received detailed study, probably because little can be said without the benefit of Singularity Theory. (Indeed, classical kinematics has surprisingly little to say about multiparameter spatial motions, for just that reason.) And even those coupler surfaces which have been studied exhibit only the simplest types of singularity, such as the cross-cap. It would be of value to understand the mechanical significance of the more degenerate types of singularity discussed in this paper.

We are concerned solely with the monogerm singularities which may appear on trajectories of generic motions. The multigerm singularities, while clearly important for a complete understanding of this situation, have not yet been completely listed. (A partial classification appears in [5].) In this paper we refer to the existing list of smooth map monogerms from the plane to space obtained in [9]. Some of the analyses of their unfoldings (the $\mathcal{A}$-simple germs on the list) appear in [1] and [2]. However, we believe the analysis of the $\mathcal{A}$-unimodular family $P_3(c)$ to be new.

2 Transversality & Classification

First we establish notations. Let $E(p)$ denote the Lie group of proper rigid motions of $\mathbf{R}^p$. By an *n-dimensional motion* of $\mathbf{R}^p$ we mean a smooth mapping $\lambda : N \to E(p)$, where N is a smooth manifold of dimension n. That yields a smooth mapping $M_\lambda : N \times \mathbf{R}^p \longrightarrow \mathbf{R}^p$ defined by $(t, w) \mapsto \lambda(t)(w)$: and for any fixed choice of $w \in \mathbf{R}^p$ it yields a smooth mapping $M_{\lambda,w} : N \longrightarrow \mathbf{R}^p$ defined by $t \mapsto \lambda(t)(w)$, which we refer to as the *trajectory* of w under λ. We think of M_λ as a p-parameter family of trajectories. Given positive integers r and k this induces a multijet extension ${}_rj^kM_{\lambda,w} : N^{(r)} \longrightarrow {}_rJ^k(N, \mathbf{R}^p)$, and since $M_{\lambda,w}$ depends smoothly on w that yields a mapping

$${}_rj^kM_\lambda : N^{(r)} \times \mathbf{R}^p \longrightarrow {}_rJ^k(N, \mathbf{R}^p).$$

Theorem 2.1 ([3]) *Let $\mathcal{S}$ be a finite stratification of ${}_rJ^k(N, \mathbf{R}^p)$. The set of n-dimensional motions $\lambda : N \longrightarrow E(p)$ with ${}_rj^kM_\lambda$ transverse to $\mathcal{S}$ is residual in $C^\infty(N, E(p))$, endowed with the Whitney C^∞ topology.*

In this situation there is a codimensional restriction on the relevant strata of $\mathcal{S}$, which we need to make precise. Let X be an $\mathcal{A}$-invariant smooth submanifold of ${}_rJ^k(n, p)$, giving rise in a natural way to an $\mathcal{A}$-invariant smooth submanifold Y of ${}_rJ^k(N, \mathbb{R}^p)$. Suppose that ${}_rj^kM_\lambda$ is transverse to $\mathcal{S}$, and that Y is one of the strata. Then a necessary condition for the pull-back of Y under ${}_rj^kM_\lambda$ to be non-void is that Y has codimension $\leq rn + p$, the dimension of the domain. However an easy argument using local triviality of the multijet bundle shows that the codimensions of X, Y in their respective multijet spaces differ by $(r-1)p$. Thus the condition on X is that its codimension should be $\leq 2p + r(n-p)$. Given n, p the guiding principle for classification is to list strata in the multijet space up to this figure. In particular, for a generic motion non-stable $\mathcal{A}$-simple multigerms of trajectories will be of $\mathcal{A}_1$-codimension $\leq p$. For potential applications to robotics the important cases are $p = 2$ (of planar motions) and $p = 3$ (of spatial motions) where it is realistic to expect complete solutions. In this paper we are concerned solely with the case $n = 2$, $p = 3$ so need to list strata up to codimension $6 - r$: in particular, for the case $r = 1$ of monogerms we are concerned solely with strata of codimension ≤ 5. Our first step is to check that for a residual set of motions, monogerms of trajectories are given by existing classifications.

Lemma 2.1 *For a residual set of motions λ, singular monogerms of trajectories have corank 1; and they are either $\mathcal{A}$-simple of $\mathcal{A}_e$-codimension ≤ 3, or (in the notation of [10]) of type P_3.*

Proof Take X to be the subset of $J^k(2,3)$ comprising k–jets with zero 1–jet. Then X is $\mathcal{A}$-invariant, smooth, and of codimension 6, so (by the above) cannot be met transversely by the jet–extension. That establishes the first statement. However, the listing in [11], contains all *strata* of codimension ≤ 6; P_3 is the only non–simple singularity for which the corresponding stratum in the jet–space has codimension ≤ 5.

Table 1, taken from [10], lists all monogerms of $\mathcal{A}$–simple germs of $\mathcal{A}_e$–codimension ≤ 3, plus the unimodular family P_3. For each type the subscript indicates the $\mathcal{A}_e$–codimension. The third column gives the degree d of $\mathcal{A}$–determinacy, and the columns headed $C(f)$, $T(f)$ and $\mu(\widetilde{D^2}/\mathbf{Z}_2)$ give known integer invariants of the associated *complex* germs. C is the number of cross–caps which appear in a generic unfolding; T gives the number of triple points; and $\mu(\widetilde{D^2}/\mathbf{Z}_2)$ is a geometric invariant [7] arising from the double point curve. The germ of type $P_3(c)$ is finitely $\mathcal{A}$–determined if and only if the modulus c does not assume one of the four exceptional values $c = 0$, $c = \frac{1}{2}$, $c = 1$ or $c = \frac{3}{2}$: and the family of these germs is $\mathcal{A}$–unimodular. Note in particular that $P_3(c)$ is weighted homogenous: indeed if x, y are assigned the weights 2, 1 then the components have weighted degrees 2, 3, 4.

The specializations for the real monogerms in Table 1 are summarized in Figure 01 below. If each occurrence of the superscript $*$ is replaced either with a $+$ or with a $-$ we obtain a correct specialization diagram. For instance each of C_3^+ and C_3^- specialize to S_2, B_2^+ and B_2^-.

$$\begin{tikzcd}
 & & B_3^* \arrow[d] & \\
 & C_3^* \arrow[r] \arrow[d] & B_2^* \arrow[d] & \\
S_3^* \arrow[r] & S_2 \arrow[r] & S_1^* \arrow[r] & S_0 \\
 & P_3(c) \arrow[r] \arrow[u] & H_2 \arrow[u] & \\
 & & H_3 \arrow[u] &
\end{tikzcd}$$

Figure 01

Name	Normal Form	d	$C(f)$	$T(f)$	$\mu(\widetilde{D^2}/\mathbf{Z}_2)$
S_0	(x, y^2, xy)	2	1	0	0
S_1^+	$(x, y^2, y^3 + x^2y)$	3	2	0	0
S_1^-	$(x, y^2, y^3 - x^2y)$	3	2	0	0
S_2	$(x, y^2, y^3 + x^3y)$	4	3	0	0
S_3^+	$(x, y^2, y^3 + x^4y)$	4	4	0	0
S_3^-	$(x, y^2, y^3 - x^4y)$	4	4	0	0
B_2^+	$(x, y^2, x^2y + y^5)$	5	2	0	2
B_2^-	$(x, y^2, x^2y - y^5)$	5	2	0	2
B_3^+	$(x, y^2, x^2y + y^7)$	7	2	0	4
B_3^-	$(x, y^2, x^2y - y^7)$	7	2	0	4
C_3^+	$(x, y^2, xy^3 + x^3y)$	4	3	0	2
C_3^-	$(x, y^2, xy^3 - x^3y)$	4	3	0	2
H_2	$(x, y^3, xy + y^5)$	5	2	1	0
H_3	$(x, y^3, xy + y^8)$	8	2	2	0
$P_3(c)$	$(x, xy + y^3, xy^2 + cy^4)$	5	3	1	2

Table 1: Monogerms of Codimension ≤ 3

3 Conditions for Cross–Caps and Triple Points

Given $f : X \to Y$ finite and analytic, we consider the set $M_k(f)$ of points in Y whose pre–image comprises $\geq k$ points, counting multiplicities. Following the method in [12], this can be done by looking at the scheme structure of the $M_k(f)$ using the Fitting ideals of the coherent $\mathcal{O}_Y$–module $f_*\mathcal{O}_X$. The $M_k(f)$ are the zero sets of the Fitting ideals, $F_k(\mathcal{O}_X)$, so we first construct the ideals from a presentation of $f_*\mathcal{O}_X$, using the following algorithm. We describe the algorithm for a germ $f : \mathbf{C}^n, 0 \to \mathbf{C}^{n+1}, 0$: if f is finite it will produce the double point curve and the triple points provided they exist.

(1) Choose a projection $\pi : \mathbf{C}^{n+1} \to \mathbf{C}^n$ such that $\tilde{f} = \pi \circ f$ is still finite (this is Noether normalization and is always possible). We may suppose that $f(x) = (\tilde{f}(x), f_{n+1}(x))$.

(2) Find generators $g_1 = 1,\ g_2, \ldots,\ g_h$ for $\mathcal{O}_{\mathbf{C}^n,0} = \mathcal{O}_n$ (source) over $\mathcal{O}_n$ (target) via $\tilde{f}^*$ (by the Weierstrass Preparation Theorem these can always be found).

(3) Find the (unique) $\alpha_j^i \in \mathcal{O}_n$, $1 \leq i, j \leq h$ such that $g_j f_{n+1} = \sum_i (\alpha_j^i \circ \tilde{f}) g_i$.

(4) Noting that $f_{n+1} = x_{n+1} \circ f$, and letting λ_j^i be defined by the relations below, we can view the equations as relations $\lambda_j^1.g_1 + \ldots + \lambda_j^h.g_h = 0$ amongst the g_i over $\mathcal{O}_{n+1}$.

$$\lambda_j^i = \begin{cases} \alpha_j^i \circ \pi & i \neq j \\ \alpha_i^i \circ \pi - x_{n+1} & i = j. \end{cases}$$

(5) Then the matrix $\lambda = (\lambda_i^j)$ is the presentation matrix of $f_* \mathcal{O}_n$ over $\mathcal{O}_{n+1}$

$$\mathcal{O}_{n+1}^h \xrightarrow{\lambda} \mathcal{O}_{n+1}^h \longrightarrow f_* \mathcal{O}_n \longrightarrow 0$$

The k^{th} *Fitting ideal* of $f_* \mathcal{O}_n$, $F_k(f_* \mathcal{O}_n)$ is defined to be the ideal in $\mathcal{O}_{n+1}$ generated by all $(h-k) \times (h-k)$ minors of λ for $0 \leq k < h$. Denote the zero set of $F_k(f_* \mathcal{O}_n)$ by $M_k(f)$. Then:

- $f^* M_0(f)$ gives the pre–image
- $f^* M_1(f)$ gives the double point curve in the source, i.e. the pre–images of double points.
- $f^* M_2(f)$ gives the pre–images of triple points.

When $f^{-1}(\mathbf{C}^{n+1})$ is Gorenstein, $M_1(f)$ may be found by deleting the first column and hth row of the presentation matrix, and considering only the resulting $(h-1) \times (h-1)$ determinant – all others are in the ideal generated by this. A particular case is provided by

Lemma 3.1 *If* $f : \mathbf{C}^2, 0 \longrightarrow \mathbf{C}^3, 0$ *is given by* $f(x,y) = (x, y^2, yp(x,y^2))$ *then* $p(x,y^2) = 0$ *is the equation of the double point curve in the source.*

Proof In this case we can assume Gorenstein. We take $\tilde{f}(x,y) = (x,y^2)$. The generators of $\mathcal{O}_2$ (source, coords (x,y)) over $\mathcal{O}_2$ (target , coords (X,Y)) are 1, y. Then $Z.1 = yp(X,Y)$, $Z.y = Yp(X,Y)$ and the presentation matrix is

$$\lambda = \begin{pmatrix} -Z & p(X,Y) \\ Yp(X,Y) & -Z \end{pmatrix}$$

so $M_1(f)$ is given by $p(X,Y) = 0$, i.e. by $p(x,y^2) = 0$.

Note that Lemma 3.1 applies to all the singularities we wish to analyse, apart from H_2, H_3 and P_3. Excluding these for now, our approach is to consider the double point curve in the source for each singularity and then to take its image under the fold map $(x,y) \mapsto (x,y^2)$. This gives the curve of self–intersection of the singular surface representing the image of the stable mapping $f_t : \mathbf{C}^2 \to \mathbf{C}^3$. By [10] we know that if f has the form $f(x,y) = (x, r(x,y), s(x,y))$ then the co-ordinates of the cross–caps are given by the solutions of the equations

$$\frac{\partial r}{\partial y}(x,y) = 0 : \quad \frac{\partial s}{\partial y}(x,y) = 0.$$

In the particular case when $r(x,y) = y^2$, $s(x,y) = yp(x,y^2)$ the cross-caps are given by the solutions of the single polynomial equation $p(x,0) = 0$.

A few words are in order concerning the application of the above to *real* germs. For cross-caps, we have the following result [11].

Proposition 3.1 *Let $f : \mathbf{R}^2, 0 \to \mathbf{R}^3, 0$ be an $\mathcal{A}$-finite germ of corank 1. Then there exist arbitrarily small real deformations of f exhibiting $C(f)$ real cross-caps.*

However the situation concerning triple points is rather different. We do have the following result of Marar & Mond [8].

Proposition 3.2 *Let $f : \mathbf{R}^2, 0 \to \mathbf{R}^3, 0$ be a finitely determined map-germ with corank 1 at 0. Then if f is from the H_k series of singularities $T(f)$ real triple points will be exhibited under some small real deformation. In particular, there exist real deformations of H_2 exhibiting exactly one real triple point, and of H_3 exhibiting exactly two real triple points.*

4 The Unfoldings

In this section we use the methods of §3 to analyze the $\mathcal{A}_e$-versal unfoldings (in Table 2 below) of the germs in Table 1; in particular we determine conditions on the unfolding parameters giving rise to the maximum number $C(f)$ of cross-caps and the maximum number $T(f)$ of triple points. Note that in view of the remarks made in §3 the double point curves for the S, B and C types are obtained by removing the factor y from the third component of the unfolding. Pictures of the unfoldings for the S, B and C types appear in [1], with detailed analyses in [2]. The method of §3 has the advantage that it applies to *all* examples, and renders the mechanics for the S, B and C types particularly simple.

THE TYPE S_1^+. The double point curve is $y^2 + x^2 + a$, so a circle for $a < 0$, a point for $a = 0$, and empty for $a > 0$: in the target that yields the pictures illustrated in Figure 02. Cross caps are the intersections with the x-axis, so there are two for $a < 0$ and none for $a > 0$. In the intermediate case $a = 0$ the surface has a cuspidal cross-section.

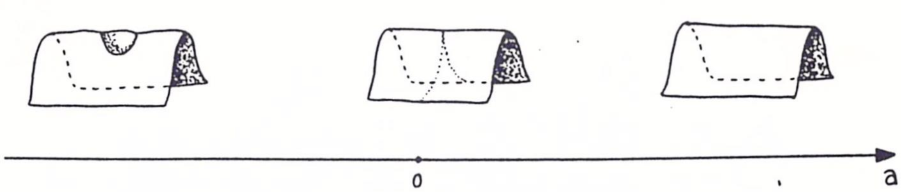

Figure 02

Type	Versal Unfolding	Double Point Curve
S_1^+	$(x, y^2, y^3 + x^2y + ay)$	$y^2 + x^2 + a$
S_1^-	$(x, y^2, y^3 - x^2y + ay)$	$y^2 - x^2 + a$
S_2	$(x, y^2, y^3 + x^3y + ay + bxy)$	$y^2 + x^3 + a + bx$
S_3^+	$(x, y^2, y^3 + x^4y + ay + bxy + cx^2y)$	$y^2 + x^4 + a + bx + cx^2$
S_3^-	$(x, y^2, y^3 - x^4y + ay + bxy + cx^2y)$	$y^2 - x^4 + a + bx + cx^2$
B_2^+	$(x, y^2, x^2y + y^5 + ay + by^3)$	$x^2 + y^4 + a + by^2$
B_2^-	$(x, y^2, x^2y - y^5 + ay + by^3)$	$x^2 - y^4 + a + by^2$
B_3^+	$(x, y^2, x^2y + y^7 + ay + by^3 + cy^5)$	$x^2 + y^6 + a + by^2 + cy^4$
B_3^-	$(x, y^2, x^2y - y^7 + ay + by^3 + cy^5)$	$x^2 - y^6 + a + by^2 + cy^4$
C_3^+	$(x, y^2, xy^3 + x^3y + ay + by^3 + cxy)$	$xy^2 + x^3 + a + by^2 + cx$
C_3^-	$(x, y^2, xy^3 - x^3y + ay + by^3 + cxy)$	$xy^2 + x^3 + a + by^2 + cx$
H_2	$(x, y^3 + ay, xy + y^5 + by^2)$	curve of degree 6
H_3	$(x, y^3 + ay, xy + y^8 + by^2 + cy^5)$	curve of degree 14
$P_3(c)$	$(x, xy + y^3 + ay, xy^2 + cy^4 + by + dy^3)$	

Table 2: Versal Unfoldings for the Germs in Table 1

THE TYPE S_1^-. The double point curve is $y^2 - x^2 + a$, so a hyperbola symmetric about the x-axis for $a < 0$, a line-pair for $a = 0$, and a hyperbola symmetric about the y-axis for $a > 0$: in the target that yields the pictures illustrated in Figure 03. There are no cross-caps for $a < 0$, and two for $a > 0$. In the intermediate case $a = 0$ the surface has a cuspidal cross-section.

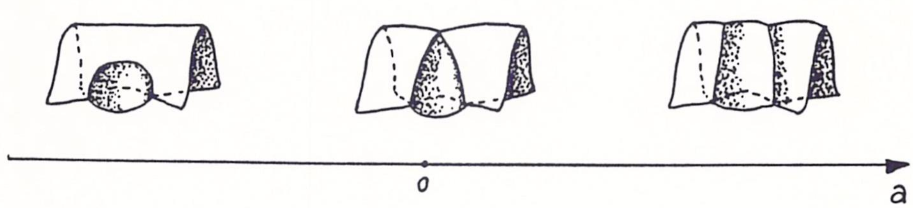

Figure 03

THE TYPE S_2. The double point curve is the cubic $y^2 + x^3 + a + bx$. Write Δ for the discriminant of $x^3 + a + bx$: then $\Delta = 0$ is a cuspidal cubic in the (a, b)-plane. 'Outside' this curve we have one real root, hence one cross-cap: and 'inside' we have three real roots, and hence three cross-caps. On the discriminant curve we obtain an acnodal cubic for $a > 0$, and a crunodal cubic for $a < 0$. The changes in the double point curve, its folding, and the resulting surface are illustrated in Figure 04.

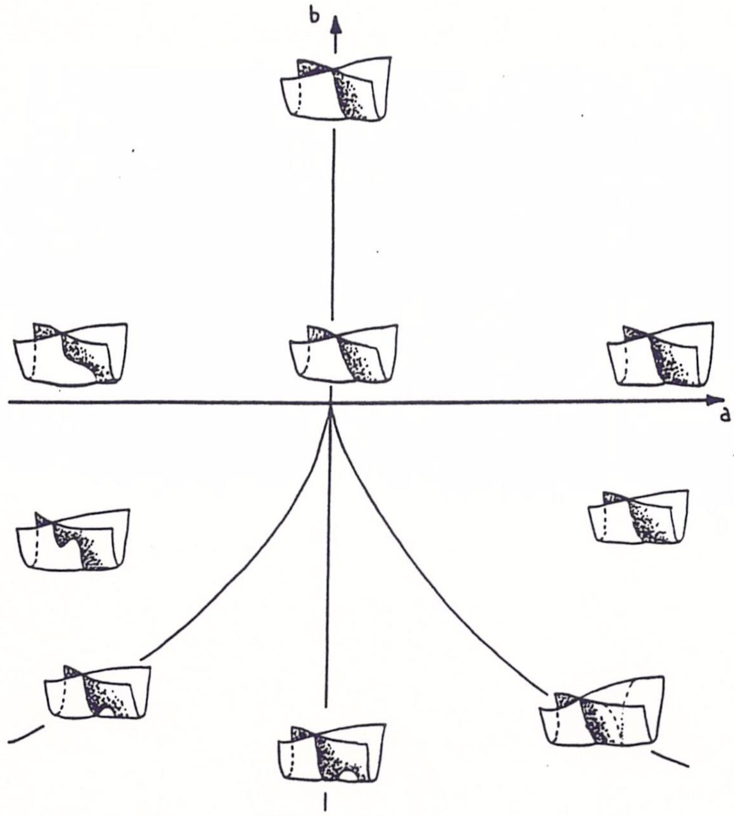

Figure 04

THE TYPE S_3^+. The double point curve is the quartic $y^2+x^4+a+bx+cx^2$. Write Δ^+ for the discriminant of $x^4+a+bx+cx^2$: then $\Delta^+=0$ is the swallowtail surface in (a,b,c)–space, illustrated in Figure 05, together with the corresponding forms of the double point curve, and the corresponding image surfaces exhibiting zero, one, two, three or four cross–caps.

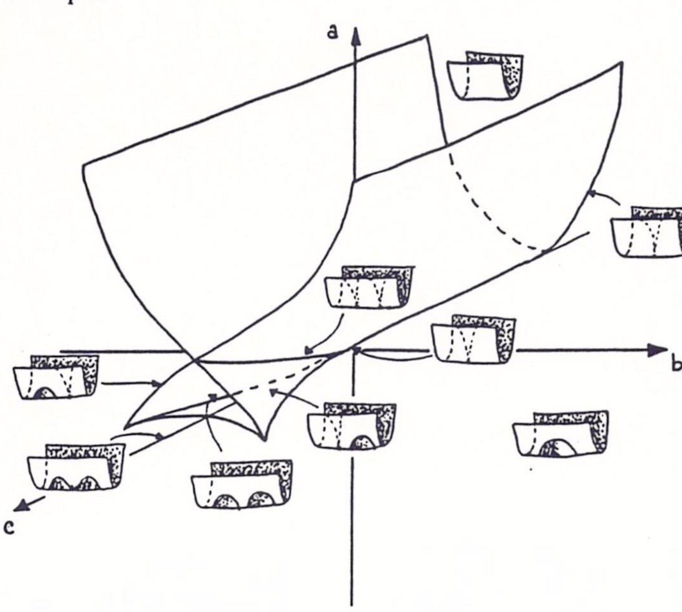

Figure 05

THE TYPE S_3^-. The double point curve is the quartic $y^2 - x^4 + a + bx + cx^2$. Write Δ^- for the discriminant of $-x^4 + a + bx + cx^2$. Then the zero set of Δ^- is obtained from that of Δ^+ by central reflexion. That yields the illustrations in Figure 06.

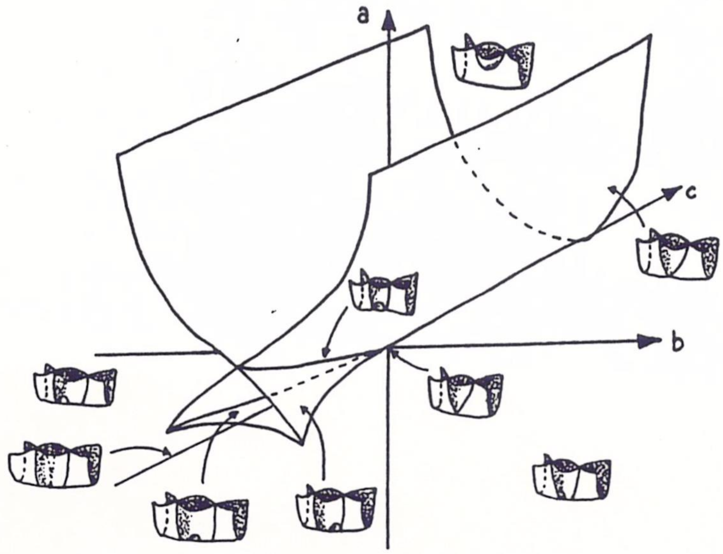

Figure 06

THE TYPE B_2^+. The double point curve is the quartic $x^2 + y^4 + a + by^2$. When $a < 0$ the polynomial $y^4 + a + by^2$ has 2 distinct real zeros: when $a = 0$ it has 1 or 3 according as $b \geq 0$ or $b < 0$: when $a > 0$ and $b \geq 0$ it has no zeros: and when $a > 0$ and $b < 0$ it has 0, 2 or 4 according as $b^2 - 4a$ is positive, zero or negative. The resulting forms of the double point curve, its folding, and the image surface are illustrated in Figure 07. We notice that at certain unfolding points the double point curve has self-tangencies: this is related to the fact that in this case $\mu(\widetilde{D}^2/\mathbf{Z}_2)$ is non-zero [7].

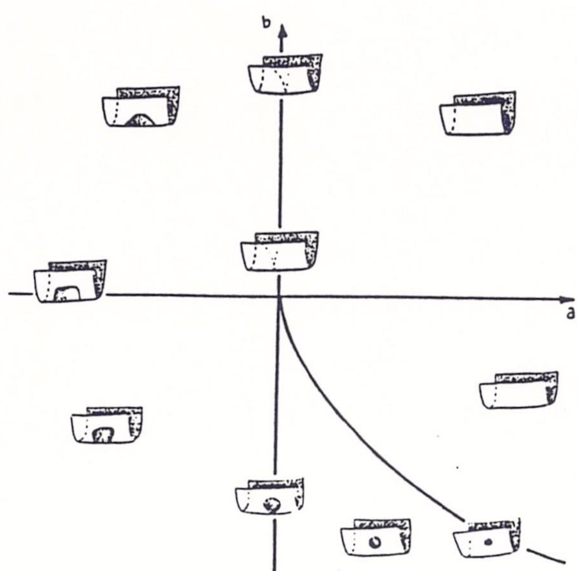

Figure 07

THE TYPE B_2^-. The double point curve is the quartic $x^2 - y^4 + a + by^2$. The analysis here is virtually identical to that for the type B_2^+, with the various forms of the double point curve, its folding, and the image surface illustrated in Figure 08. Again the double point curve has self-tangencies.

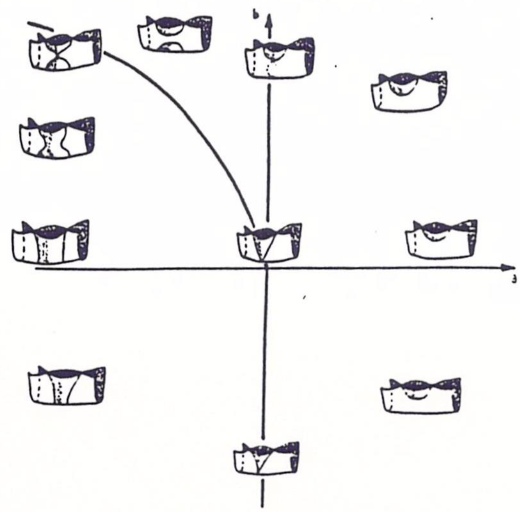

Figure 08

THE TYPE B_3^+. The double point curve is the sextic $x^2 + y^6 + a + by^2 + cy^4$. We obtain cross-caps when $x^2 + a = 0$: thus there are 2 for $a < 0$ and none for $a > 0$. The discriminant Δ of the polynomial $y^6 + a + by^2 + cy^4$ of degree 3 in y^2 has zero-set a quartic surface in (a, b, c)-space

$$\Delta = 27a^2 - 18abc + 4ac^3 - b^2c^2 + 4b^3$$

where $b < 0$, or $b \geq 0$, $c < 0$ and $c^2 - 3b > 0$. This surface is 'half' a cuspidal edge with non-zero torsion. Combining it with the plane $a = 0$ we get the bifurcation set illustrated in Figure 09. Note again that here $\mu(\widetilde{D}^2/\mathbf{Z}_2)$ is non-zero.

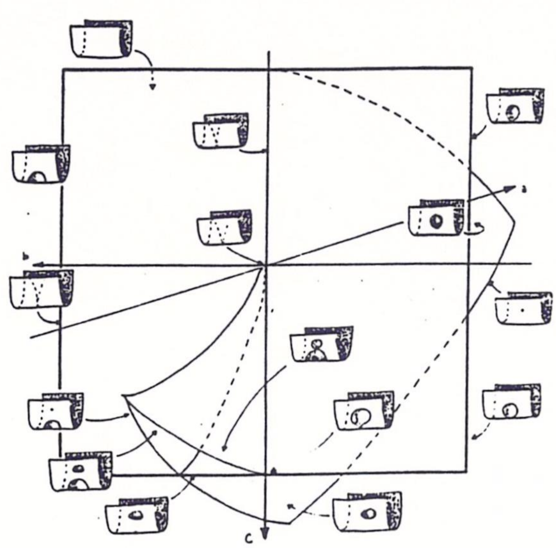

Figure 09

THE TYPE B_3^-. Again the double point curve is the sextic $x^2+y^6+a+by^2+cy^4$. and the analysis is very similar to that of the type B_3^+. The bifurcation set is shown in Figure 10.

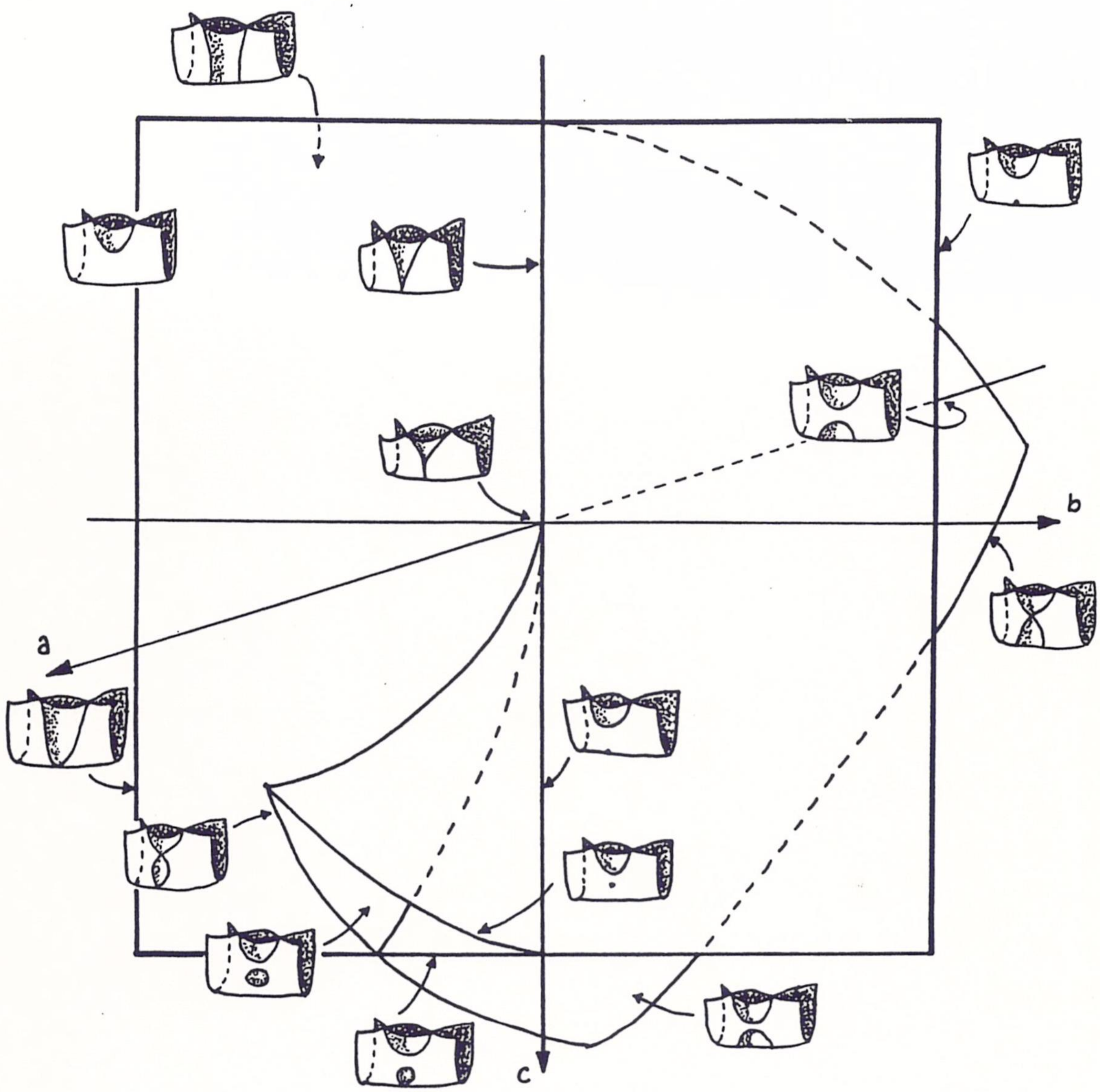

Figure 10

THE TYPE C_3^+. The double point curve here is $y^2(x+b)+x^3+cx+a=0$. We obtain cross-caps when $x^3+cx+a=0$, so there are three when $27a^2 < -4c^3$, two when $27a^2 = -4c^3$ and one otherwise. This part of the bifurcation set is a cuspidal edge. When $x = b$ we have the cusp catastrophe surface, $b^3 - bc + a = 0$, which forms the other part of the bifurcation set. On this surface the double point curve becomes reducible. The two surfaces are tangent. The bifurcation set is illustrated in Figure 11. Note that the form of the bifurcation set obtained using the methods of §3 is not identical to that obtained in [13]. The two are in fact diffeomorphic.

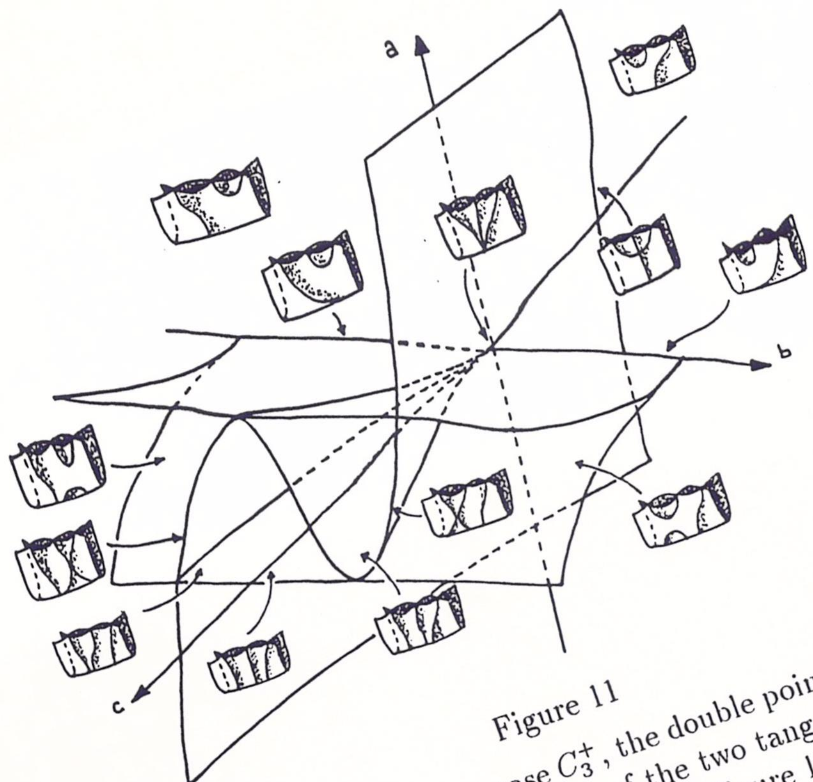

Figure 11

THE TYPE C_3^-. Similar to the case C_3^+, the double point curve is $y^2(x+b)-x^3+cx-a=0$, and the bifurcation set consists of the two tangential surfaces $27a^2=4c^3$ and $a=b(c-b^2)$. The bifurcation set is shown in Figure 12.

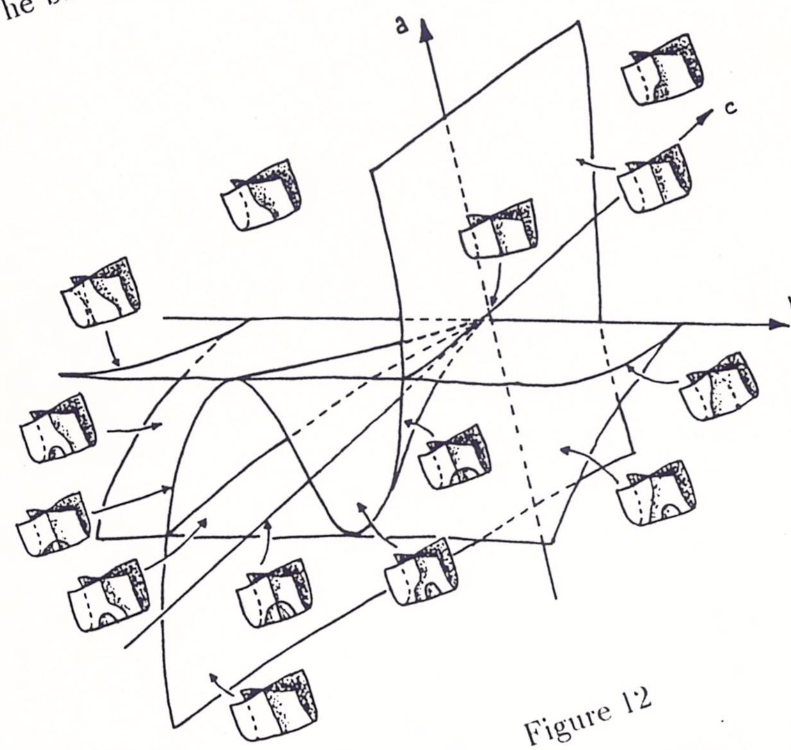

Figure 12

THE TYPE H_2. In this case we cannot use Lemma 3.1 to find the double point curve – we must go back to the method of finding a presentation matrix and calculating the relevant determinant. Taking $\tilde{f}(x,y) = (x, y^3 + ay)$, the presentation matrix with respect to generators 1, y and y^2 is

$$\lambda = \begin{pmatrix} -Z - aY & X + a^2 & Y + b \\ Y(Y+b) & -Z - 2aY - ab & X + a^2 \\ Y(X + a^2) & Y^2 + bY - aX - a^3 & -Z - 2aY - ab \end{pmatrix}$$

The resulting double point curve is a sextic, whose equation is easily written down, but is not very informative. It is easier to find the cross-caps in the image using

$$\frac{\partial}{\partial y}(y^3 + ay) = \frac{\partial}{\partial y}(xy + y^5 + by^2) = 0$$

yielding $y = \pm\sqrt{-a/3}$. There are two cross-caps when $a < 0$, and none otherwise.

To determine the unfolding parameters giving triple points, consider the variety generated by the 1×1 minors of the presentation matrix. The relevant ideal is

$$\langle xy + y^5 + by^2 + ay^3 + a^2y,\ x + a^2,\ y^3 + ay + b \rangle$$

The last equation gives a condition on a and b, since if we require three pre-images of a point in the image it must have three real roots. That yields the condition $27b^2 < -4a^3$. So the bifurcation set consists of this cusp and the line $a = 0$, illustrated in Figure 13.

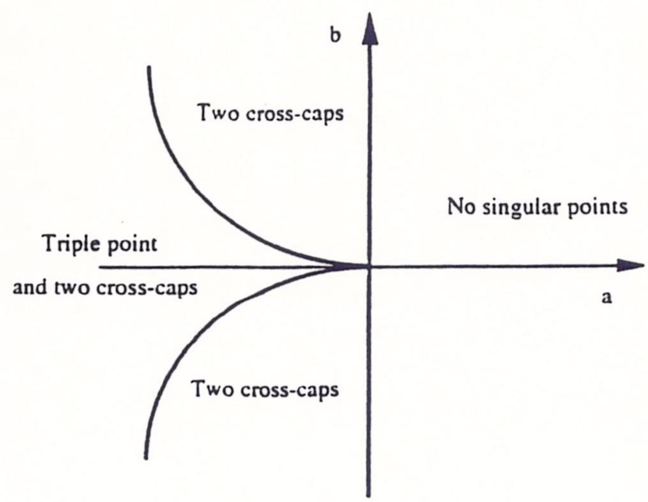

Figure 13

THE TYPE H_3. Taking $\tilde{f}(x,y) = (x, y^3 + ay)$ the presentation with respect to $1, y, y^2$ is given by.

$$\begin{pmatrix} -Z - 2aY^2 - caY & 3a^2Y + X + ca^2 & Y^2 - a^3 + b + cY \\ Y(Y^2 - a^3 + b + cY) & -Z - 3aY^2 - 2acY + a^4 - ab & 3a^2Y + X + a^2c \\ Y(3a^2Y + a^2c + X) & Y(Y^2 - 4a^3 + b + cY) & -Z + a^4 - 2acY - 3aY \end{pmatrix}$$

The double point curve has degree 14. It is simpler to find the cross-caps by solving

$$\frac{\partial}{\partial y}(y^3 + ay) = \frac{\partial}{\partial y}(xy + y^8 + by^2 + cy^5) = 0$$

giving $3y^2 + a = 0$, and an equation for x in terms of y. Thus there are two cross-caps in the image for $a < 0$ and none otherwise.

Conditions for triple points (of which we expect to see at most two) are given by the vanishing of the 1×1 minors of the presentation matrix, yielding

$$\begin{aligned} 0 &= -xy - y^8 - 2ay^6 - cy^5 - 4a^2y^4 - y^2(b + 2a^3) \\ 0 &= 3a^2y^3 + 3a^3y + x + a^2c \\ 0 &= y^6 + 2ay^4 + cy^3 + a^2y^2 + acy - a^3 + b. \end{aligned}$$

As in the case of H_2, we use the last of these to give conditions for triple points. For two triple points, this sextic must have six distinct real roots, so its discriminant D must be positive. A MAPLE computation gives D as a polynomial in a, b, c. It is more illuminating to change to co-ordinates A, B, C defined by $A = -3a$, $B = 31a^3 - 27b$, $C = 2c$ in which

$$D = (B^2 - A^3C^2)\left\{\frac{1}{4}C^2 + \frac{16}{729}A^3 + \frac{4}{17}B\right\}$$

defining a reducible sextic surface depicted in Figure 14. One component is a folded umbrella, and the other is a non-singular cubic surface meeting the umbrella tangentially along a sextic space curve. The complement of the discriminant surface splits (A, B, C)-space into a number of connected components giving rise various bifurcations, analyzed in detail in [5]. For $A > 0$ there are two cross-caps in the image of the unfolding, otherwise none. In the small region between the two components of the discriminant surface there are two triple points and two cross-caps in the image, bifurcating to one triple point and two cross-caps (H_2) and then no triple points and two cross-caps (S_1), or to two distinguished points and two cross-caps (also S_1). Figure 15, taken from [6], illustrates the topological construction of the image of an H_3 singularity.

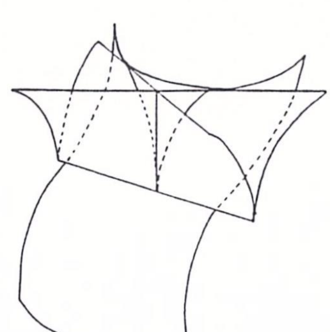

Figure 14

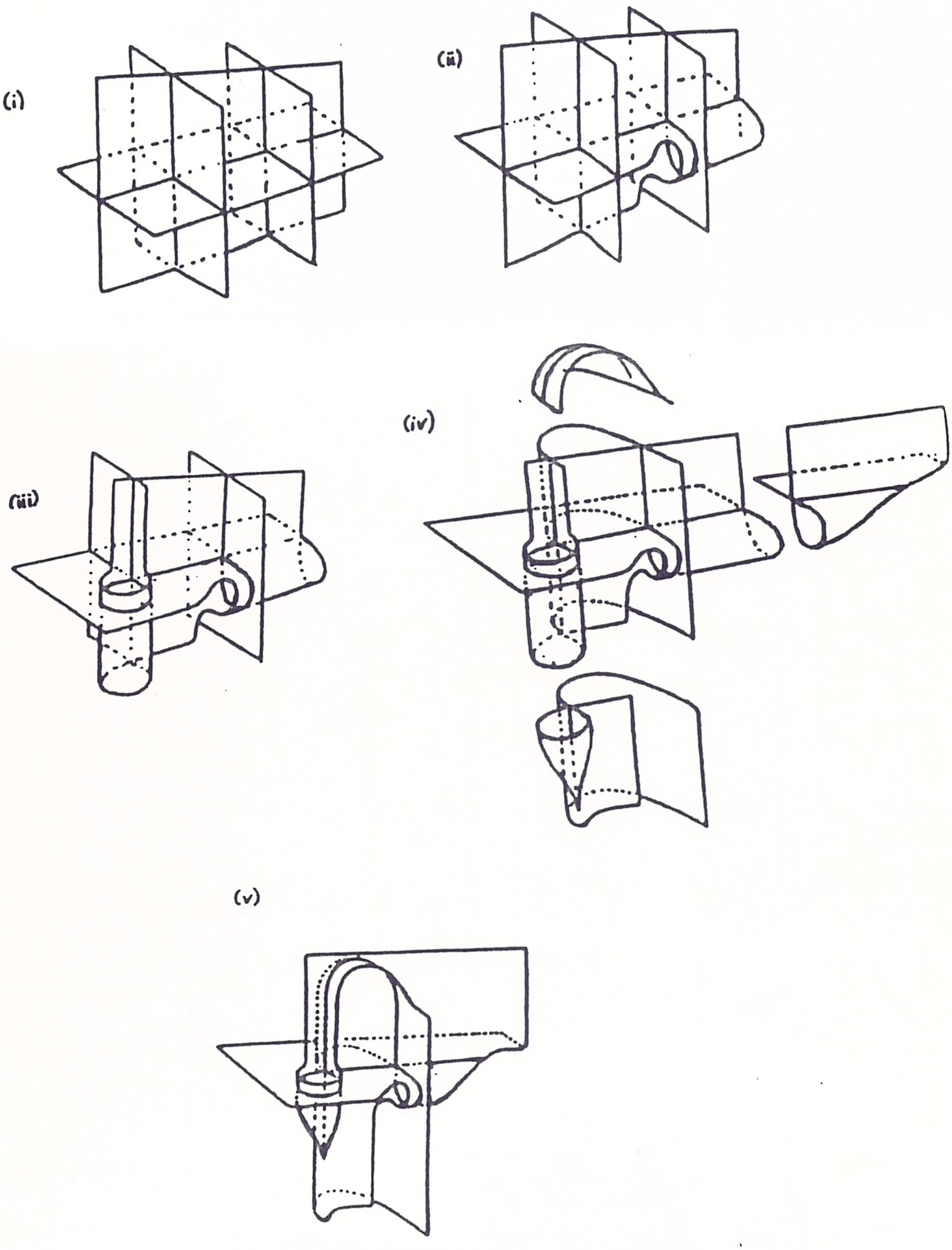

Figure 15

THE TYPE $P_3(c)$. This unimodular family requires rather more analysis than the preceding monogerms. Recall first that there are four exceptional values of the modulus c, namely the values $c=0$, $c=\frac{1}{2}$, $c=1$ and $c=\frac{3}{2}$ for which the germ fails to be $\mathcal{A}$-determined. (By a result in [7] that is equivalent to the germ at the origin of the double point curve being finitely $\mathcal{K}$-determined.) It turns out that there are two further values of c, namely $c=\frac{4}{3}$ and $c=2$ which play a special role.

For the versal unfolding of P_3 given in Table 2 we wish first to determine the subsets of the parameter space (a,b,c,d) giving rise to cross-caps and triple points. The unfolding has the shape $f_c(x,y)=(X,X(x,y),Z(x,y))$ with $X=x$, $Y=xy+y^3+ay$, $Z=xy^2+cy^4+by+dy^3$. By the results in §3 cross-caps are given by

$$0=\frac{\partial Y}{\partial y}=x+3y^2+a \quad : \quad 0=\frac{\partial Z}{\partial y}=2xy+4cy^3+b+3dy^2$$

defining a parabola and a cubic curve in the real affine plane intersecting (in principle) in ≤ 6 points. Projectively, the cubic has a node at $(1:0:0)$ with nodal tangents $y=0$, $z=0$, and the conic has a simple point there with tangent $z=0$: there are therefore ≥ 3 intersections at infinity, hence ≤ 3 intersections in the real affine plane. More brutally, elimination of x from the above relations yields a cubic in y

$$2(2c-3)y^3+3dy^2-2ay+b=0.$$

For a fixed value of the modulus c the discriminant of this cubic defines a quartic surface in (a,b,d)–space, separating the regions giving rise to three real roots and one real root. We refer to this as the *cross-cap surface* with modulus c, and denote it CCS. Explicitly, it has equation

$$3\{3(2c-3)b+ad\}^2=-(9bd-4a^2)\{4a(2c-3)+3d^2\}.$$

Next, we turn our attention to triple points. The presentation matrix of the unfolding is easily checked to be

$$\begin{pmatrix} -Z+dY & H(X,Y) & G(X) \\ YG(X) & -Z+dY-(X+a)G(X) & H(X,Y) \\ YH(X,Y) & YG(X)-(X+a)H(X,Y) & -Z+dY-(X+a)G(X) \end{pmatrix}$$

where $G(X)=(1-c)X-ac$, $H(X,Y)=-dX+cY+(b-ad)$. By the theory of §3, triple points are given by the vanishing of all entries in the matrix, which happens if and only if $0=dY-Z$, $0=G(X)$, $0=H(X,Y)$, equivalent to the single cubic in y

$$c(1-c)y^3+acy+\{(1-c)b-ad\}=0.$$

For a fixed value of the modulus c the discriminant of this cubic defines a quartic surface in (a,b,d)–space, separating the regions giving rise to three real roots and one real root. We refer to this as the *triple point surface* with modulus c, and denote it TPS. Explicitly, it has equation

$$-27(1-c)\{(1-c)b-ad\}^2 = 4c^2a^3.$$

We ask now for more detailed information about the CCS and the TPS. It helps to observe that the natural $\mathbf{R}^*$ action on the unfolding space for $P_3(c)$ restricts to one on the CCS and TPS, with a, b, d having respective weights 2, 3, 1. The orbits provide natural foliations of these surfaces, the general orbit being a twisted cubic, possibly degenerating. The singular sets of both surfaces are cuspidal edges, corresponding to those points (a,b,d) for which the cubics in y are perfect cubes. For instance the cubic in y giving rise to the CCS is a perfect cube $(sy+t)^3$ when $2(2c-3)=s^3$, $3d=3s^2t$, $-2a=3st^2$ and $b=t^3$: the first relation defines s in terms of c, and then the remaining relations provide an explicit parametrisation of a twisted cubic. However, the cubic in y giving rise to the TPS can only be a perfect cube when $a=b=0$, so the cuspidal edge for the TPS is the d–axis, which (incidentally) is contained in the CCS. On the other hand an obvious calculation verifies that the cuspidal edge for the CCS only intersects the TPS at the origin, save for the unique value $c=\frac{4}{3}$ of the modulus when the whole edge is contained in the TPS.

In view of the above comments, if the CCS and TPS intersect at a point then they do so along the whole $\mathbf{R}^*$–orbit. It is therefore sufficient to understand the intersections of the two surfaces with the plane $d=1$, yielding two cubic curves in the (a,b)–plane intersecting (in principle) in ≤ 9 points. We dub these the *cross–cap curve* and the *triple point curve* and abbreviate them to CCC and TPC. The underlying geometry of these curves is easily established. The TPC is a cuspidal cubic with cusp at the origin, and cuspidal tangent the line $a+(c-1)b=0$. Likewise, the CCC is a cuspidal cubic, with cusp at the point

$$a=\frac{-3}{4(2c-3)} \quad : \quad b=\frac{1}{4(2c-3)^2}.$$

The cusp locus is the parabola $9b=4a^2$, with the origin deleted. For $c<\frac{3}{2}$ the cusp lies in the first quadrant; for the exceptional value $c=\frac{3}{2}$ it is the point at infinity on the b–axis; and for $c>\frac{3}{2}$ it lies in the second quadrant.

Consider next the intersections of the TCP and the CCC. The origin is simple on the CCC, with tangent line $b=0$, distinct from the cuspidal tangent to the TPC, so the curves have *two* intersections there. Both (projective) curves have their unique flex at $(0:1:0)$, with inflexional tangent the line at infinity, so have *at least three* intersections at infinity. Thus we expect the curves to have *at most four* intersections (in fact 0, 2 or 4 real intersections) in the (a,b)–plane, away from the origin. More explicitly, one can rationally parametrize the TPC via the pencil of lines $b=\lambda a$ through its cusp, and substitute the results in the equation of the CCC. As expected, that yields a real quartic $q(\lambda)$. MAPLE verifies that $q(\lambda)$ has a zero discriminant, indeed that it has a repeated linear factor $\{3(c-1)(c-2)\lambda+(5c-6)\}^2$, and that the residual quadratic factor has discriminant $(2c-3)c^3$. Thus $q(\lambda)$ always has a repeated zero: for $0<c<\frac{3}{2}$ there are two further distinct zeros, and otherwise there are no further real zeros. In the former case, explicit calculation (by hand) verifies that the only non-exceptional value of c for which the repeated zero has multiplicity 3 is $c = \frac{4}{3}$. (Recall that this is the unique value of c for which the cuspidal edge on the CCS lies in the TPS.) Further the point of intersection of the CCC and the TPC corresponding to the repeated zero of $q(\lambda)$ has co-ordinates (α, β) where

$$\alpha = \frac{3(c-1)}{(c-2)^2} \qquad \beta = -\frac{(5c-6)}{(c-2)^3}.$$

(α, β) is simple on the CCC (save when $c = \frac{4}{3}$ when it is the cusp) hence a point of tangency of the two curves. Note that for the unique non-exceptional value $c = 2$ it is the point at infinity on the b–axis. More detailed analysis is required if one wishes to sketch the TCP and the CCC by hand: the series of tracings in Figure 16 were obtained using the ALGCURVE program, mentioned in the introduction.

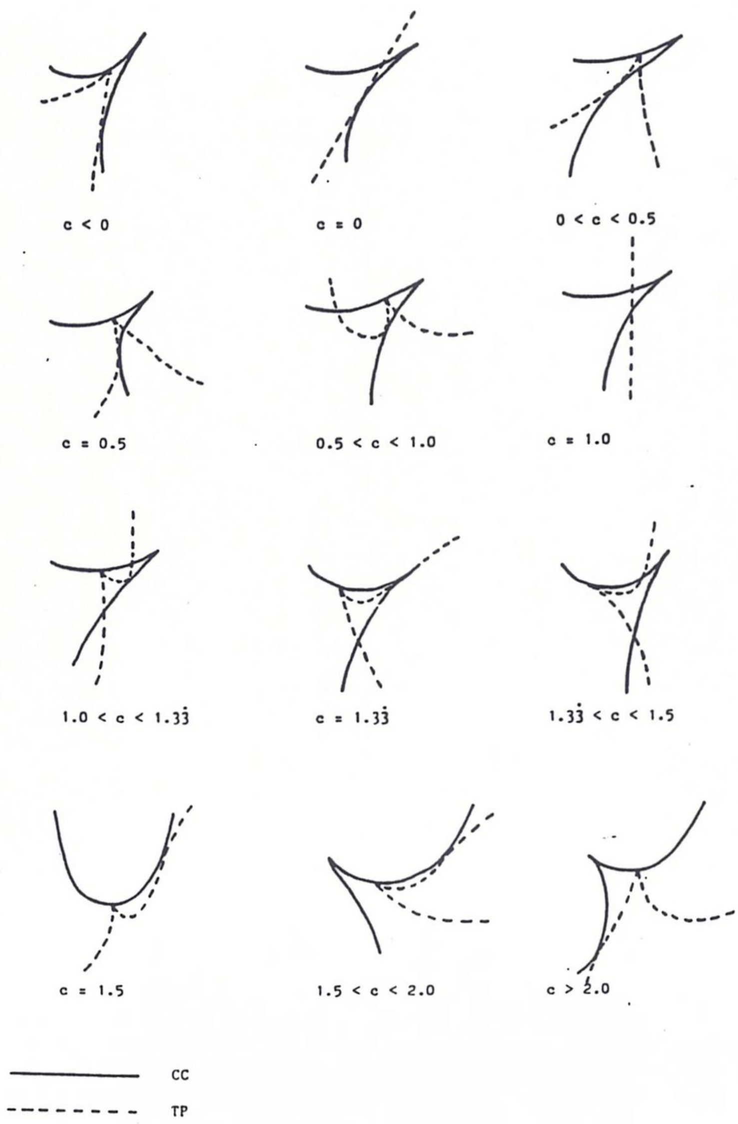

Figure 16

References

[1] Arnol'd, V. I. Singularities of Caustics and Wave Fronts, Math. Appl., 62, Kluwer Publishing Press. (1990)

[2] Bruce, J. W. and Wilkinson, T. C. Folding Maps and Focal Sets. Singularity Theory and its Applications, Springer Verlag, (1991) 63–72.

[3] Gibson, C. G. and Hobbs, C. A. Singularities of General One–Dimensional Motions of the Plane and Space. Proc. Roy. Soc. Edin., 125A, (1995), 639–656.

[4] Gibson, C. G. and Hobbs, C. A. Singularity and Bifurcation for General Two–Dimensional Planar Motions. To appear in New Zealand Jour. Math. (1995).

[5] Hobbs, C. A. Kinematic Singularities of Low Dimension. Ph.D. Thesis, University of Liverpool. (1993).

[6] Marar, W. L. Mapping Fibrations and Multiple Point Schemes. Ph.D. Thesis, University of Warwick. (1989).

[7] Marar, W. L. and Mond, D. M. Q. Multiple Point Schemes for Corank 1 Maps. J.London Math. Soc., 39(2), (1989), 553–567.

[8] Marar, W. L. and Mond, D. M. Q. Real Map Germs with Good Perturbations. To appear in Topology. (1995)

[9] Mond, D. M. Q. Classification of Certain Singularities and applications to Differential Geometry, Ph.D. Thesis, University of Liverpool. (1982)

[10] Mond, D. M. Q. On the Classification of Germs of Maps from $\mathbf{R}^2$ to $\mathbf{R}^3$. Proc. London Math. Soc., 50 (3), (1985), 333–369.

[11] Mond, D. M. Q. Some Remarks on the Geometry and Classification of Germs of Maps from Surfaces to 3–space. Topology, 26 (3), (1987), 361–383.

[12] Mond, D. M. Q. and Pellikaan, R. Fitting Ideals and Multiple Points of Analytic Mappings. Algebraic Geometry and Complex Analysis, Springer Verlag, (1987), 107–161.

[13] Wilkinson, T. The Geometry of Folding Maps, Ph.D. Thesis, University of Newcastle. (1991)

NOTAS DO ICMSC

SÉRIE MATEMÁTICA

031/95 LUCAS, L. A., MANZOLI-NETO, O. and SAEKI, O., *An unknotting theorem for $S^p \times S^q$ embedded in S^{p+q+2}*

030/95 BIASI, C. and GODOY, S.M.S., *On the aleatory variable* $Y_n = 10^n X - [10^n X]$ *for large n*

029/95 CARVALHO, A. N., CHOLEWA, J. W. and DLOTKO, T., *Examples of global attractors in parabolica problems*

028/95 LUCAS, L. A., MANZOLI-NETO, O. and SAEKI, O., *A generalization of Alexander's torus theorem to higher dimensions*

027/95 BIASI, C. and GONÇALVES, D. L., *Equivalent conditions for n-equivalences module a class C of groups*

026/95 CARVALHO, A. N. and HINES, G., *Lower semicontinuity of unstable manifolds for gradient systems*

025/95 GARCIA, R.A.; MOCHIDA, D.; FUSTER, C.R. and RUAS, M. A. S., *Inflection points and topology of surfaces in 4-space*

024/95 CASSAGO JR., H.; GODOY, S. M.; and TÁBOAS, P.Z., *Periodic solutions of planar differential equations with two delays*

023/94 ZANI, S. L., *Two-weight norm inequalities for maximal functi ons on homogeneous spaces and boundary estimates*

022/94 LABOURIAU, I. S. and RUAS, M. A. S., *Singularities of equations of Hodgkin-Huxley type*